Proceedings of the 17th World Congress
The International Federation of Automatic Control
Seoul, Korea, July 6-11, 2008

Modeling of Voltage Hysteresis and Relaxation of HEV NiMH Battery

Yutaka Ota, Masaru Sakamoto, Rei Kiriake, Takashi Kobe, and Yoshihiro Hashimoto

Nagoya Institute of Technology
Gokiso, Showa, Nagoya, Aichi, 4668555, JAPAN
Tel&Fax: +81-52-735-5389 e-mail: yota@nitech.ac.jp

Abstract: SOC (State Of Charge) estimation based battery management is important for HEV (Hybrid Electric Vehicle) applications. There are many difficulties in SOC estimation of HEV NiMH (Nickel Metal Hydroxide) batteries, for example, gassing at charge, self discharge, hysteresis and relaxation of OCV (Open Circuit Voltage), memory effect during charge-discharge cycling, and so on. In this paper, a modeling of hysteresis and relaxation of HEV NiMH battery is investigated. Model structure is simple, and model parameters are fitted by using voltage and current measurements. Accuracy of modeling is evaluated by using experimental results of 7.2V, 6.5Ah NiMH battery module.

1. INTRODUCTION

Battery is one of the key components for HEV. Improvement of fuel efficiency is accomplished by charge from regenerative braking and then discharge at starting and accelerating, for which engine efficiency is low. HEV battery is required the charge-discharge cycling with high power in a short time. SOC estimation based battery management is essential to accept sufficient power from the regenerative braking, to supply sufficient power to the electrical drive, and to prevent over charge or discharge.

SOC can be estimated by integrating charge-discharge current. This method is called as coulomb counting. However if charge-discharge cycle is increased, estimation error is accumulated by gassing and self discharge. On the other hands, it is well known that OCV and SOC have relationship based on Nernst equation. SOC estimation is expected by using Nernst equation at the timing when OCV can be measured or estimated. As a peculiar problem for HEV NiMH battery, there is voltage hysteresis phenomenon, in which measured OCV after charge (discharge) is higher (lower) than estimated OCV by Nernst equation (Ta et al., 1999, Srinivasan et al., 2001, Motloch et al., 2002). This voltage hysteresis has been modeled by adding simple voltage modification term to Nernst equation (Pan et al., 2002, Verbrugge et al., 2004), by using a SOC-dependent voltage source including hysteresis (Bohlen et al., 2006, Thele et al., 2006). These method needs history information whether battery has been charged or discharged. And SOC and OCV is no longer one-to-one relationship.

In this paper, to express voltage hysteresis of HEV NiMH battery, layers model concerning Nickel active materials is proposed. A forward voltage of diode between surface layer and inside layer of Nickel active materials produce the SOC distribution. OCV of each layer is defined by Nernst equation. And measured battery voltage is reflected by OCV of surface layer. Of course, proposed model can provide high power for HEV application because the diode has no internal resistance. Besides voltage hysteresis, voltage relaxation is expressed as equalization between surface layer and relaxation layer with higher internal resistance because voltage relaxation slowly progress with time constant from few minutes to few hours. After charge-discharge, internal charge exchange flows according to potential difference between surface layer and relaxation layer. The model parameters are capacitor ratio of three layers, two internal resistances, and forward voltage of diode. Complicated kinetic or cell geometrical parameters are not used in proposed model. SOC distribution between layers is original concept, and new battery management scheme considering SOC distribution is expected.

2. VOLTAGE HYSTERESIS AND RELAXATION

Some experiments were operated to investigating OCV hysteresis. HEV Ni-MH battery module, which nominal voltage is 7.2V and battery capacity is 6.5Ah, is used. Fig.1 shows an example of experiments. First of all, battery module is charged with 7.2Ah, which is considered as nearly full charge taking into account of gassing at charge process. Relaxation and hysteresis after discharge is measured during one hour after discharge, and battery is refreshed by discharge until 6V cut-off voltage. Relaxation and hysteresis after charge is also measured during one hour after charge, and then battery is refreshed. Capacity of charge is from 0.65Ah (10% of 6.5Ah) to 5.2Ah (80% of 6.5Ah), and capacity of discharge is from 1.3Ah (20% of 6.5Ah) to 5.85Ah (90% of 6.5Ah) every 0.65Ah (10% of 6.5Ah). Charge-discharge current is 1C rate (6.5A). Fig.1 shows 3.25Ah (50% of 6.5Ah) case. Hysteresis is confirmed by different OCV values after 3.25Ah charge from refreshed condition and after 3.25Ah discharge from full charged condition. OCV measurements just after charge-discharge and after relaxation at each SOC are summarized in Fig.2. Horizontal axis shows real value of electric capacity estimated by coulomb counting of discharge current during refresh after charge or discharge.

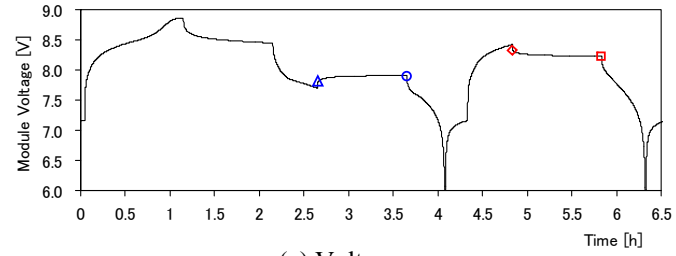

(a) Voltage

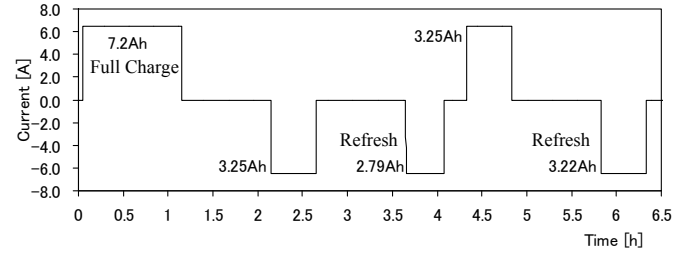

(b) Current

Fig.1. Time responses of voltage, current at charge-discharge.

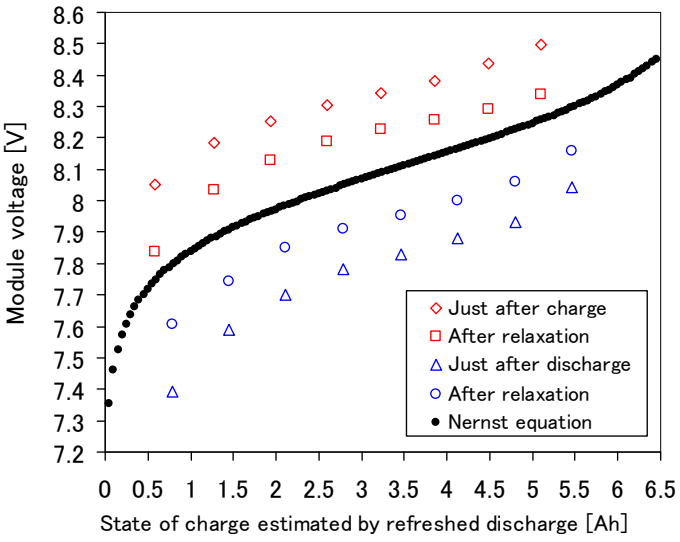

Fig.2. OCV just after charge-discharge, OCV after relaxation, and OCV defined by Nernst equation at each electric capacity estimated by coulomb counting during refresh.

In Fig.2, OCV defined by Nernst equation (V_{NiMH}) is calculated based on SOC as follows.

$$V_{Ni} = V_{Nieq} + \frac{RT}{F}\ln\left(\frac{SOC}{C - SOC}\right) \quad (1)$$

$$V_{MH} = V_{MHeq} \quad (2)$$

$$V_{NiMH} = 6\left(V_{Ni} + V_{MH}\right) \quad (3)$$

Where, R is universal gas constant, R=8.314472. F is faraday constant, F=96485.3415. T is temperature of battery module, and is preserved to be around 298.15K by thermostatic chamber. C is battery capacity. V_{Nieq} is standard potential of nickel electrode, V_{Nieq}=0.427V (Bratsch, 1989). V_{MHeq} is standard potential of metal hydroxide electrode, V_{MHeq}=0.9263V (Wu et al., 2001, Barvarisi et al., 2006). OCV after relaxation show the hysteresis loop around Nernst curve, and behave as battery capacity is smaller than 6.5Ah. The more depth of charge (discharge) is, the more width of relaxation is. It is obvious that complex characteristics of hysteresis and relaxation cannot be expressed by adding simple voltage modification term to Nernst equation.

3. BATTERY MODELING

3.1 Model Structure

Fig.3 shows a schematic diagram of NiMH battery and a proposed model during charge. Nickel active materials are divided to three layers, and distribution of each layer is considered. Surface layer is connected with inside layer by diode, and total battery capacity (C) is divided into capacity of surface layer (x) and capacity of inside layer (C-x). The surface layer is firstly charged through internal resistance (r_{int}), which is an aggregate of resistance of current collector, electrolyte, and electrodes, from power supply. If potential difference between surface and inside exceeds the forward voltage of diode (ε), charge current flow into inside layer.

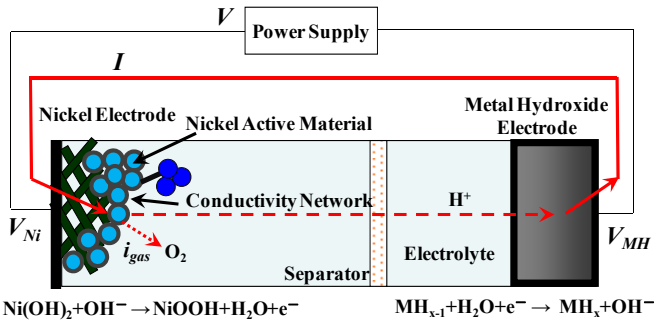

(a) Schematic diagram of NiMH battery

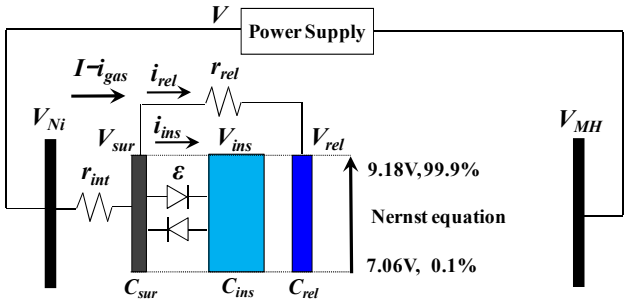

(b) Equivalent three layers model

Fig.3. NiMH battery model.

This voltage distribution between surface and inside is a mechanism of voltage hysteresis. Measured voltage (V_{NiMH}) is equivalent to sum of OCV of small surface layer (V_{sur}) and voltage drop in internal resistance. So battery is appeared to be smaller than battery capacity. Relaxation layer is non cobalt-coating active materials, and its electric conduction is low. If potential difference between surface and relaxation layer is occurred, voltage of surface and relaxation is equalled flowing internal current through higher resistance (r_{rel}). This equalization is a mechanism of voltage relaxation.

Model equations are expressed by using state variables of each layer (SOC, current, and voltage), charge-discharge current, and battery voltage as follows.

$$\frac{d\mathrm{SOC}_{sur}}{dt} = \left(I - i_{gas}\right) - i_{ins} - i_{rel} \tag{4}$$

$$\frac{d\mathrm{SOC}_{ins}}{dt} = i_{ins} \tag{5}$$

$$\frac{d\mathrm{SOC}_{rel}}{dt} = i_{rel} \tag{6}$$

$$i_{gas} = i_{gas\,0} \exp\left\{\alpha_1\left(V_{sur} - V_0\right) + \alpha_2\left(T - T_0\right)\right\} \tag{7}$$

$$i_{ins} = \begin{cases} 0 & (|V_{sur} - V_{ins}| < 0) \\ i_{ins} & (|V_{sur} - V_{ins}| \geq 0) \end{cases} \tag{8}$$

$$i_{rel} = \frac{V_{sur} - V_{rel}}{r_{rel}} \tag{9}$$

$$r_{rel} = \begin{cases} \beta_1 + \beta_2 \ln\left(\dfrac{\mathrm{SOC}_{rel}}{C_{rel}}\right) & (I < 0) \\ \beta_3 i_{gas} & (I > 0) \end{cases} \tag{10}$$

$$V_{sur} = 6\left\{V_{Nieq} + V_{MHeq} + \frac{RT}{F}\ln\left(\frac{\mathrm{SOC}_{sur}}{C_{sur} - \mathrm{SOC}_{sur}}\right)\right\} \tag{11}$$

$$V_{ins} = 6\left\{V_{Nieq} + V_{MHeq} + \frac{RT}{F}\ln\left(\frac{\mathrm{SOC}_{ins}}{C_{ins} - \mathrm{SOC}_{ins}}\right)\right\} \tag{12}$$

$$V_{rel} = 6\left\{V_{Nieq} + V_{MHeq} + \frac{RT}{F}\ln\left(\frac{\mathrm{SOC}_{rel}}{C_{rel} - \mathrm{SOC}_{rel}}\right)\right\} \tag{13}$$

$$V = V_{sur} + r_{int} I \tag{14}$$

Eq.(7) shows gassing current (Bohlen et al., 2006), which increase according to increase of battery voltage during charge process. V_0 is oxygen evolution voltage of nickel electrode, V_0=1.23*6=7.38V. T_0 is reference temperature of battery module, T_0=298.15K. i_{gas0}, α_1, and α_2 are adjusting parameters.

In Eq.(10), deterioration of relaxation resistance in low SOC region is introduced as a SOC dependent function. And deterioration of relaxation resistance is also occurred in high SOC region at charge because of gas evolution near the conductivity network. β_1, β_2, and β_3 are adjusting parameters.

In relaxed initial condition, OCV of surface layer is equalled to that of relaxation layer. Substituting measured battery voltage to Eq.(11) and Eq.(13), initial SOC is determined. Initial SOC of inside layer is adjusted as its OCV is within $\pm\varepsilon$ on Eq.(12). Firstly, the state variables are computed assuming that current don't flow into inside layer. If potential difference between surface and inside exceeds the forward voltage of diode (ε), current flows into inside layer by following equations.

$$\frac{d\mathrm{SOC}'_{sur}}{dt} + \frac{d\mathrm{SOC}'_{ins}}{dt} = \left(I - i_{gas}\right) - i_{rel} \tag{15}$$

$$V'_{sur} = V'_{ins} + \varepsilon \tag{16}$$

Considering Nernst equations about V'_{sur} and V'_{ins}, Eq.(15) and Eq.(16) become simultaneous equations about SOC'_{sur} and SOC'_{ins}. Finally, state variable of all layers are re-calculated.

3.2 Parameter fitting

Fig.4 shows an OCV measurement during relaxation after charge. The internal resistance (r_{int}) is delivered from voltage build-up at just after discharge. Now, the state just after discharge use suffix, 0, and the state after relaxation use suffix, 1. Following three OCV relationships are considered.

1. Just after discharge, OCV of inside layer (V_{ins0}) is sum of OCV of surface layer (V_{sur0}) and forward voltage of diode (ε).
2. After relaxation, OCV of relaxation layer (V_{rel1}) is equalled to OCV of surface layer (V_{sur1}).
3. During relaxation, OCV of inside layer is not change, that is, OCV of inside layer just after discharge (V_{ins0})) is equalled to that after relaxation (V_{ins1}).

Because OCV of surface layer (V_{suf0}, V_{sur1}) can be measured, V_{ins0}, V_{ins1}, V_{ins0}, and V_{rel1} are calculated by using above relationship, and SOCs are calculated by using Eq.(11)-(13). Finally, total electric capacity after relaxation is summarized as follows.

$$\mathrm{SOC}_{total\,1} = \mathrm{SOC}_{sur\,1} + \mathrm{SOC}_{ins\,1} + \mathrm{SOC}_{rel\,1} \tag{17}$$

Eq.(17) include the model parameters, ε, C_{sur}, C_{ins}, C_{rel}. These parameters can be optimized by using voltage relaxation measurements at each case shown in Fig.2. Objective function is sum of squared error of total electric capacities and real values of electric capacity estimated by coulomb counting during refresh. Result of parameter fitting is summarized in Fig.5. Each plot stand around a diagonal line, and appropriate parameter covering wide electric capacity range, which is equal to SOC range, is confirmed.

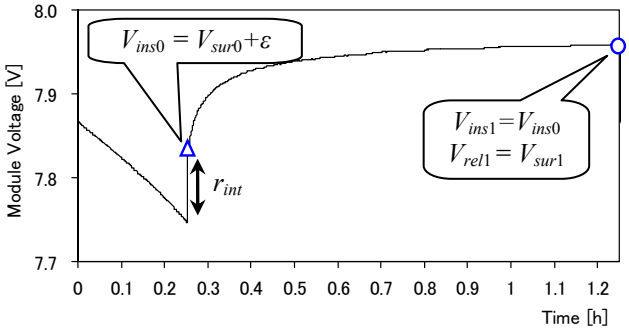

Fig.4. OCV measurement during relaxation after discharge.

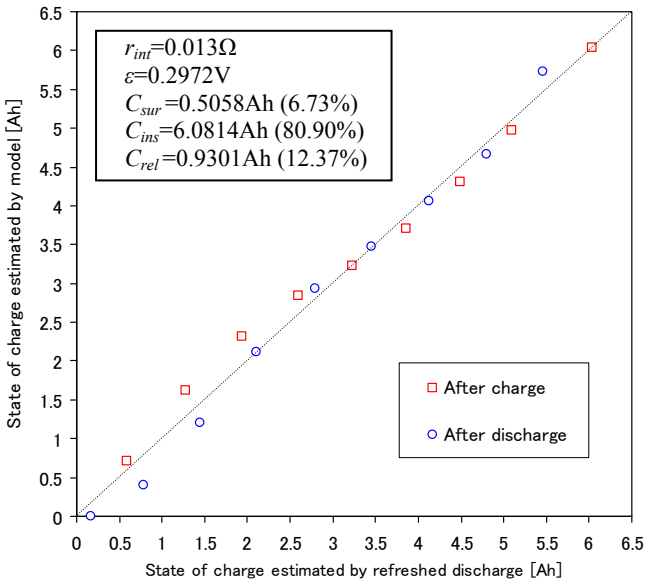

Fig.5. Results of fitting of main parameters.

3.3 Model Simulation

Fig.6 and Fig.7 show dynamic responses during 4.55Ah discharge case and 4.55Ah charge case, respectively. Model parameters, i_{gas0}, α_1, α_2, β_1, β_2, β_3, are adjusted as expressing dynamics both during charge-discharge and during relaxation. Surface layer is firstly discharged (charged), and battery behaves as its capacity is small. If potential difference between surface and inside exceeds the forward voltage of diode (ε), current flow from (into) inside layer. Relaxation dynamics is modelled by equalization of surface and relaxation layer. Accuracy of modeling is summarized in Fig.8. It is confirmed that proposed three layer distribution model can express voltage hysteresis, relaxation, and charge-discharge dynamics over wide SOC range.

4. CONCLUSIONS

In this paper, to express voltage hysteresis and relaxation, authors proposed the three layer distribution model and parameter fitting method by using voltage measurements. Its expressiveness of complicated hysteresis and relaxation phenomenon, which is not expressed by adding simple voltage modification term to Nernst equation, was validated. Model structure is simple, and convenient SOC estimation for HEV NiMH battery is expected. A concept of SOC distribution will bring a new battery management scheme.

Relaxation layer with higher resistance was used for express voltage relaxation in this paper. It is reported an active materials which have higher resistance cause the memory effect during charge-discharge cycling (Vidts et al., 1996, Sato et al., 2001, Morishita et al., 2006). And evidence of γNiOOH/αNi(OH)$_2$ during charge-discharge cycling is actually investigated (Sac-Epee et al., 1998, Ven et al., 2006). Now, we are trying to apply our model to the memory effect by assuming relaxation layer as γNiOOH/αNi(OH)$_2$, and taking into increase and decrease mechanism.

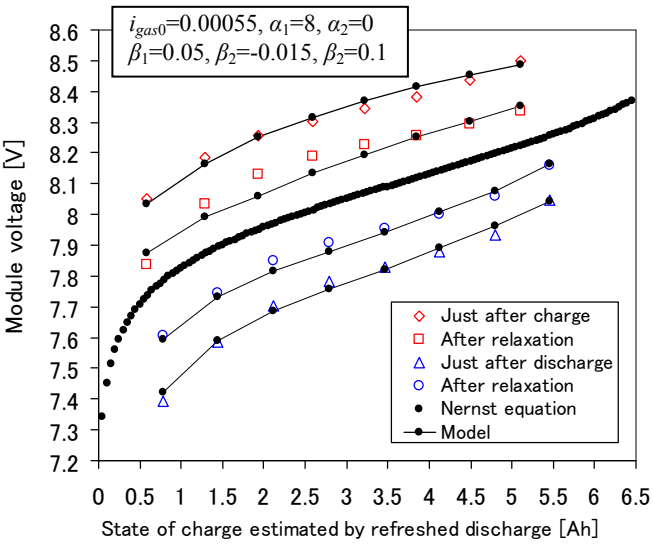

Fig.8. Modeling of voltage hysteresis and relaxation.

REFERENCES

K. P. Ta, and J. Newman (1999). Proton Intercalation Hysteresis in Charging and Discharging Nickel Hydroxide Electrodes. *J.The Electrochemical Society,* **146 (8)**, 2769-2779.

V. Srinivasan, J. W. Weidner, and J. Newman (2001). Hysteresis during Cycling of Nickel Hydroxide Active Material. *J.The Electrochemical Society,* **148 (9)**, A969-A980.

C. G. Motloch, G. L. Hunt, J. R. Belt, C. K. Ashton, G. H. Cole, T. J. Miller, C. Coates, H. S. Tataria, G. E. Lucas, T. Q. Duong, J. A. Barnes, and R. A. Sutula (2002). Implications of NiMH Hysteresis on HEV Battery Testing and Performance. *Proc.The 19th International Battery, Hybrid and Fuel Cell Electric Vehicle Symposium & Exposition*.

Y. H. Pan, V. Srinivasan, and C. Y. Wang (2002). An Experimental and Modeling Study of Isothermal Charge/Discharge Behavior of Commercial Ni-MH Cells. *J.Power Sources,* **112**, 298-306.

M. Verbrugge, E. Tate (2004). Adaptive State of Charge Algorithm for Nickel Metal Hydride Batteries Including Hysteresis Phenomena. *J.Power Sources,* **126**, 236-249.

M. Thele, M. Radin-Macukat, D. U. Sauer, O Bohlen, D. Linzen, and E. Karden (2006). Impedance-based Modeling of Electrochemical Energy Storage Devices – A Successful Implementation for NiMH Batteries used in Design Tools for Hybrid Electric Vehicles. *Proc.The 22nd International Battery, Hybrid and Fuel Cell Electric Vehicle Symposium & Exposition*.

O. Bohlen, J. B. Gerschler, D. U. Sauer, P. Birke, and M. Keller (2006). Robust Algorithms for a Reliable Battery Diagnosis -Managing Batteries in Hybrid Electric Vehicles. *Proc.The 22nd International Battery, Hybrid and Fuel Cell Electric Vehicle Symposium & Exposition*.

S. G. Bratsch (1989). Standard Electrode Potentials and Temperature Coefficients in Water at 298.15K. *J. Phys. Chem. Ref. Data,* **18 (1)**, 1-21.

P. D. Vidts, J. D. Delgado, and R. E. White (1996). A Multiphase Mathematical Model of a Nickel/Hydrogen Cell. *J.The Electrochemical Society,* **143 (10)**, 3223-3238.

Y. Sato, S. Takeuchi, and K. Kobayakawa (2001). Cause of the Memory Effect Observed in Alkaline Secondary Batteries using Nickel Electrode. *J.Power Sources,* **93**, 20-24.

M. Morishita, S. Shikimori, Y. Shimizu, A. Imasato, H. Nakamura, K. Kobayakawa, and Y. Sato (2006). The Memory Effect in the Partial Charge-Discharge Cycling of Alkaline Secondary Batteries. *J.Electrochemistry,* **74 (7)**, 532-535.

N. Sac-Epee, M. R. Palacin, A. Delahaye-Vidal, Y. Chabre, and J-M. Tarascon (1998). Evidence for Direct γ-NiOOH – β-Ni(OH)$_2$ Transitions during Electrochemical Cycling of the Nickel Hydroxide Electrode. *J. The Electrochemical Society,* **145 (5)**, 1434-1441.

A. Van der Ven, D. Morgen, Y. S. Meng, and G. Ceder (2006). Phase Stability of Nickel Hydroxides and Oxyhidroxides. *J.The Electrochemical Society,* **152 (2)**, A210-A215.

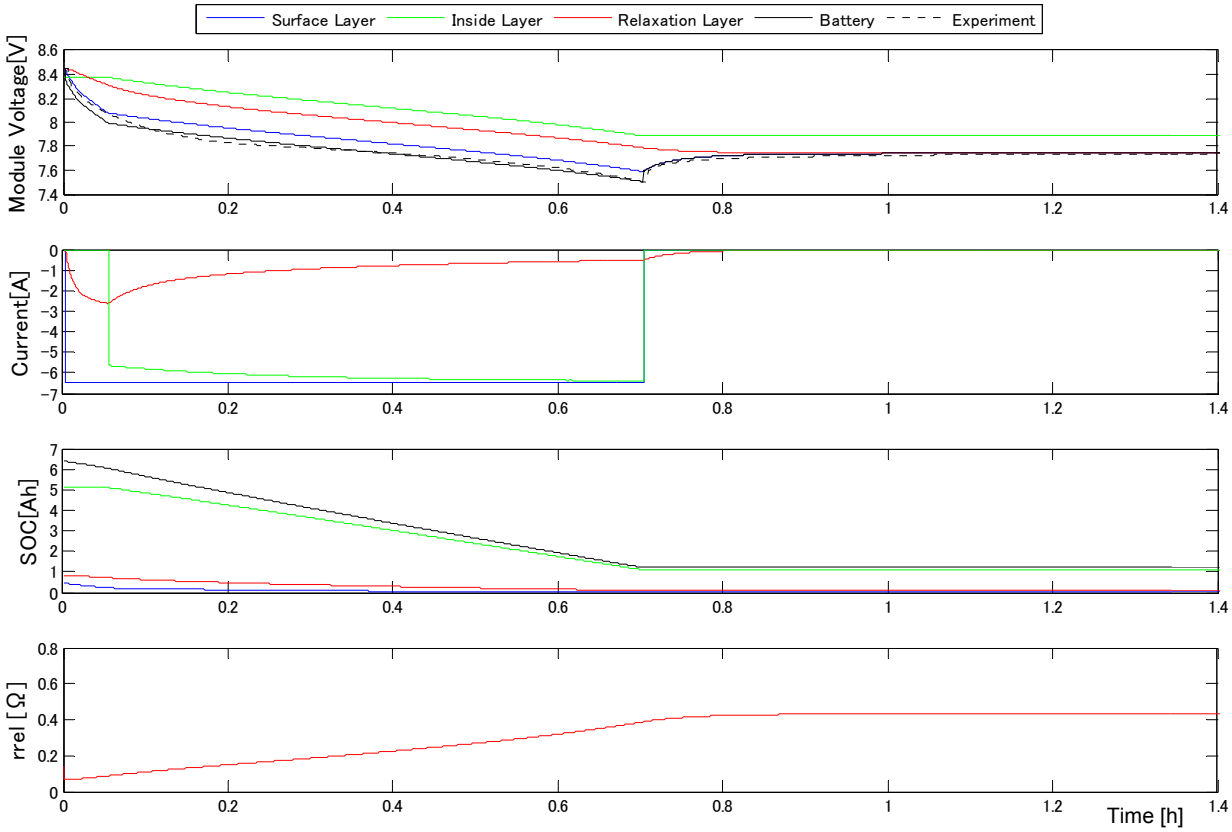

Fig.6. Simulation result at 4.55Ah discharge and relaxation.

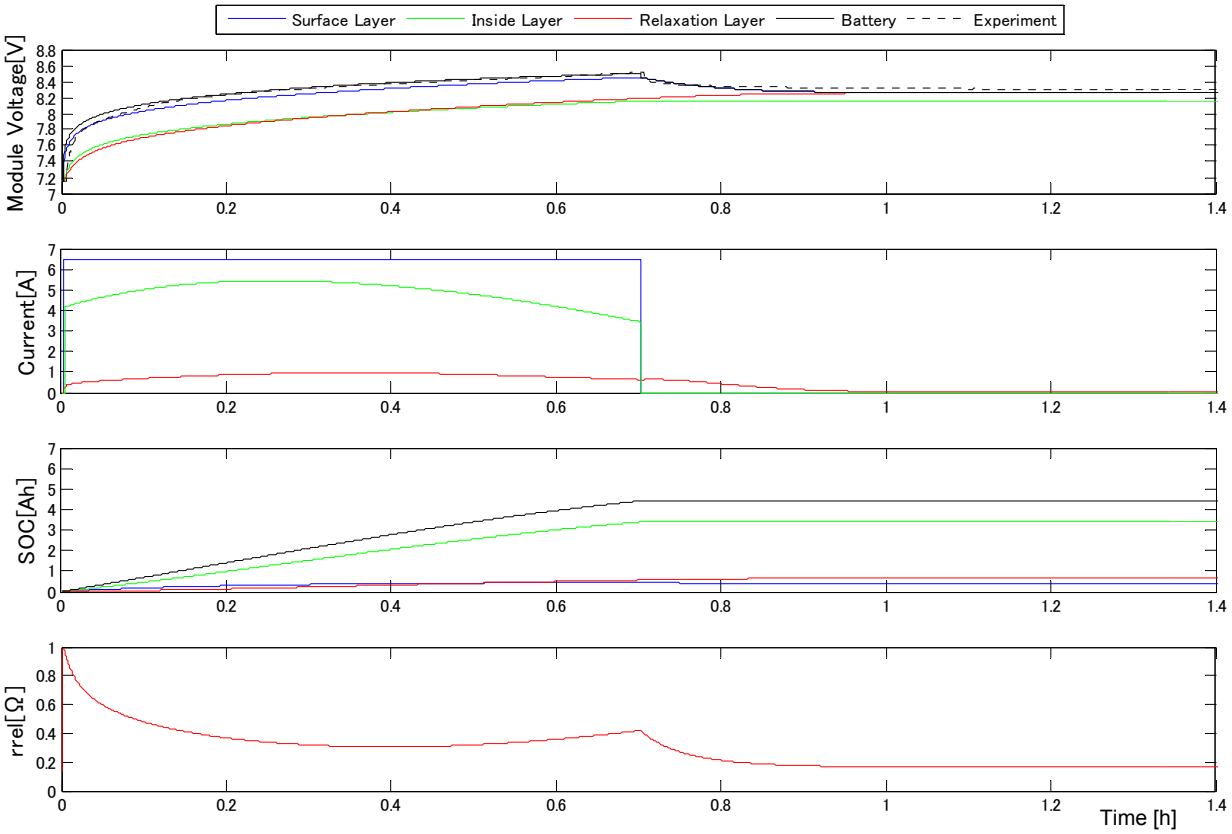

Fig.7. Simulation result at 4.55Ah charge and relaxation.